X-ray-scattering study of charge- and spin-density waves in chromium

J. P. Hill, G. Helgesen,* and Doon Gibbs
Department of Physics, Brookhaven National Laboratory, Upton, New York 11973
(Received 28 September 1994; revised manuscript received 19 December 1994)

We report an x-ray-scattering study of the incommensurate modulations in pure chromium. X-ray magnetic scattering from the spin-density wave (SDW) is observed. No resonant enhancement of the signal is obtained near the Cr K edge. On cooling through the spin-flip transition, the magnetic signal falls to zero, consistent with the polarization dependence of nonresonant magnetic scattering and the known polarization of the SDW. Charge scattering is observed at the second harmonic due to the associated charge-density wave (CDW). The intensity of the second harmonic is unchanged on cooling through the spin-flip transition. A survey of possible second-harmonic satellites reveals that a single Q state exists in the near-surface region. The amplitude of the lattice distortion is estimated to be $(\Delta_2/a)=1.5\pm0.2\times10^{-3}$, consistent with published reports. A fourth harmonic is also observed, suggesting that the CDW is not perfectly sinusoidal. The intensity of the fourth harmonic is 0.05% of the second and we find $(\Delta_4/a)=2.8\pm0.2\times10^{-5}$. The temperature dependence of the charge harmonics is found to obey mean-field scaling.

I. INTRODUCTION

Over the past ten years, the use of x-ray diffraction as a probe of magnetic ordering has grown considerably following the pioneering work of de Bregevin and Brunel.[1–3] Utilizing both nonresonant[4,5] and resonant[6–8] x-ray-magnetic-scattering techniques, a wide variety of magnetic systems has been studied, including the elemental rare-earths,[7–13] alloys[14] and thin films,[15,16] various actinide compounds,[17–19] and some transition-metal materials.[1–3,20–25] The field is briefly reviewed in Ref. 26. To date, however, the majority of materials studied have been local-moment systems. One of the motivations for the present work was to characterize magnetic scattering from an antiferromagnet in which the magnetic electrons are delocalized. Chromium was chosen as it is the canonical example of an itinerant antiferromagnet and because the spin-density-wave (SDW) state remains a fascinating problem in solid-state physics.[27] Applying the techniques of high-resolution x-ray scattering, we report the observation of x-ray magnetic scattering at $\pm Q$ and of a second harmonic to the charge-density wave (CDW) at $\pm 4Q$, where Q is the modulation wave vector.

We first briefly review the magnetic phase behavior of chromium, which forms an incommensurate, transverse SDW (TSDW) below the Néel temperature, $T_N=311$ K. The incommensurability δ, defined as the distance between the magnetic Bragg peak and the nearest commensurate reciprocal lattice point, increases smoothly on cooling from a value of $\delta=0.037$ rlu at T_N to $\delta=0.048$ rlu at $T=10$ K (1 rlu$=2\pi/a=2\times18$ Å^{-1}). The SDW attains a rms ordered moment of $\langle\mu\rangle=0.43\mu_B$ at $T=0$ K. At $T=T_{SF}=122$ K, the SDW undergoes a spin-flip transition, in which the polarization rotates to become parallel to the modulation wave vector, and forms a longitudinal SDW (LSDW). Chromium has been the subject of insensitive experimental and theoretical study over the past three decades. An excellent review is provided in Ref. 27.

The origin of the SDW in chromium, as first understood by Overhauser,[28,29] lies in the pairing of electrons with holes of opposite spin. The pairing is between momentum states separated by **Q**. When **Q** is a vector that "nests" the electron and hole Fermi surfaces, the total electronic energy is lowered and a spiral-density wave results. The ground state is formed from two spiral waves of opposite helicity, resulting in the linearly polarized SDW. For pure chromium, the nesting vector is incommensurate with the lattice and $Q=(1\pm\delta)2\pi/a$ where $a=2.88$ Å. The period of the SDW modulation is ≈27 lattice constants at T_N.[30]

Associated with the SDW ordering, there is a distortion of the lattice with twice the wave vector of the SDW. A diagram of the reciprocal space resulting from these two density waves is shown in Fig. 1. The Bragg peaks of the bcc structure are shown as filled circles. Satellites of the Bragg peaks displaced by odd multiples of Q are magnetic. Those at $\pm Q$ (open circles) were first observed by Corliss, Hastings, and Weiss[31] and Bykov *et al.*[32] using neutron scattering. Subsequently, weak third harmonics (not shown) were observed also in the neutron-diffraction pattern.[33] Even harmonics ($\pm2Q$) due to the charge-density wave[34] were first observed by Tsunoda *et al.* with x-ray diffraction[35] and subsequently also by neutron scattering.[33] Later high-resolution x-ray-scattering measurements determined the temperature dependence of the $2Q$ satellite precisely.[36]

In this paper, we report results of experiments performed largely along the $(h,0,0)$ axis. Following a discussion of the experimental details in Sec. II, we present data taken around the magnetic satellites in Sec. III. The charge scattering at $\pm2Q$ and $\pm4Q$ is discussed in Sec. IV and the amplitudes of the respective Fourier components of the density wave are estimated. In Sec. V, the temperature dependence of the harmonics is detailed, with the conclusion that mean-field scaling is observed for all harmonics. Finally, in Sec. VI the results are summarized.

0163-1829/95/51(16)/10336(9)/$06.00

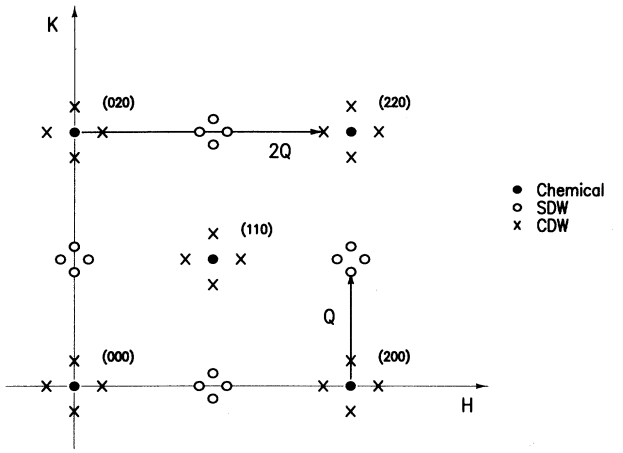

FIG. 1. Schematic of the $(h,k,0)$ plane of reciprocal space for a polydomain sample of chromium with $T<T_N=311$ K. The filled circles represent chemical Bragg peaks from the bcc structure. The open circles are the magnetic spin-density-wave satellites and the crosses the charge satellites from the second harmonic of the density modulation. The surface normals for the samples studied here are along the $(h00)$ direction.

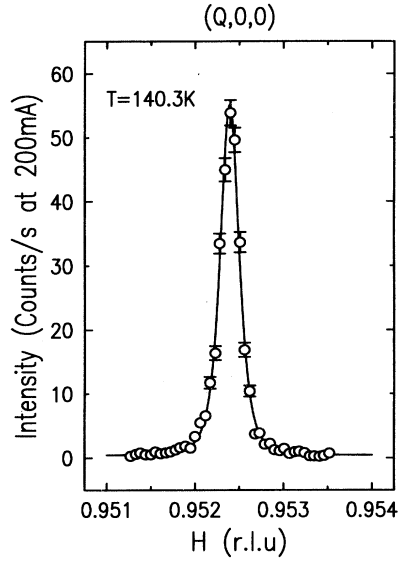

FIG. 2. Longitudinal scan through the SDW peak. These data were taken on a wiggler beamline at $E=5.91$ keV, just below the Cr K edge at $T=140.3$ K.

II. EXPERIMENTAL DETAILS

These experiments were carried out on a bending magnet beamline, X22C, and a wiggler line, X25, at the National Synchrotron Light Source. Both beamlines were configured similarly, with a toroidal mirror, placed upstream of a fixed exit double-bounce monochromator, focusing the beam horizontally and vertically at the sample position. Ge(111) and Si(111) monochromator crystals were used on the X22C and X25, respectively. A Ge(111) crystal was used to analyze the scattered beam and to reduce the background due to air scattering. In this configuration, the primary source of background originates from the sample in the form of thermal diffuse scattering and surface reflectivity. This background was significant only in the vicinity of the $2Q$ CDW satellite near T_N, where it had a count rate of 400 counts/s at beamline X25. For the purposes of this work, the essential difference between the two beamlines is the factor of 5 increase in scattered intensity obtained at the wiggler source.

The sample was sealed in a beryllium can with helium exchange gas and mounted on the cold finger of a closed-cycle helium refrigerator. Temperature stability of ± 20 mK was achieved during the course of a typical scan.

Two samples of single-crystal chromium were used in this work. Both were grown using a strain-anneal technique. Faces with a surface normal perpendicular to the (200) Bragg planes were cut and mechanically polished, leading to the observed x-ray mosaic widths of 0.03° FWHM. No differences between the two samples were observed in the results reported here.

III. MAGNETIC SCATTERING AT THE SDW SATELLITE

A longitudinal scan taken through the $(Q,0,0)$ SDW satellite position is shown in Fig. 2. These data were obtained at beamline X25 operating with an incident photon energy of $E=5.91$ keV (just below the Cr K edge) at a temperature of $T=140.3$ K. A peak of 55 counts/s is observed on a background of 0.4 counts/s.

In order to quantify the data, the longitudinal scans were fitted to a Lorentzian-squared line shape (solid line, Fig. 2) and the transverse scans were fitted to a Gaussian. These line shapes were found empirically to provide the best fits. No significance is attached to their forms. The longitudinal width of the magnetic scattering at $T=140$ K was found to be 1.26×10^{-4} rlu. Were the resolution perfect, this width would correspond to a real-space correlation length of 3600 Å. In practice, some or all of the width is due to the finite resolution and we conclude that the correlation length is well in excess of 4000 Å at $T=140$ K. On warming the sample to 309 K the width increases to 1.77×10^{-4} rlu. The transverse width is three times larger at 140 K and is dominated by the sample mosaic. It shows only a hint of broadening above $T=260$ K. Interpretation of the longitudinal broadening is complicated by the movement of the SDW satellite along the h axis, which takes the spectrometer away from the least dispersive configuration at a momentum transfer of ≈ 0.9 rlu, where the longitudinal resolution has a minimum. The CDW satellite line shape exhibits a similar broadening; but, in this case, interpretation is eased by the presence of the nearby, resolution-limited Bragg peak. We defer a discussion of the broadening to Sec. IV.

The variation of the peak position as the sample is warmed from $T=140$ K is shown in Fig. 3. Its behavior is precisely that expected for SDW scattering, based on previous neutron-scattering results.[27] It is also consistent with the variation of the CDW satellite's position measured in this sample and reported in Sec. IV.

The magnetic origin of this scattering is confirmed by the behavior of the integrated intensity obtained at $(2-Q,0,0)$ as a function of temperature, and shown in

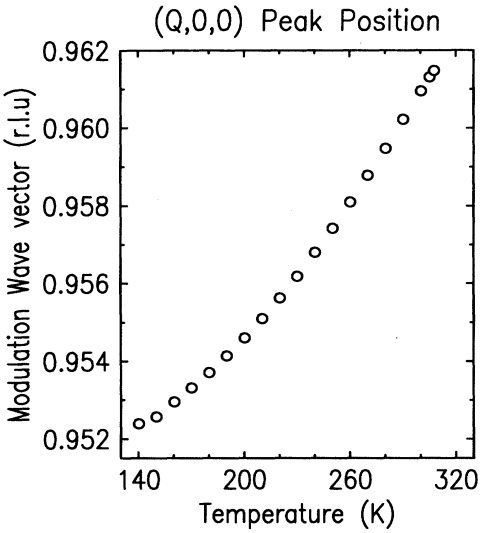

FIG. 3. The peak position of the $(Q,0,0)$ SDW peak, in units of $2\pi/a$, where a is the room-temperature lattice constant. The value corresponds precisely to a quarter of the difference between the $2Q$ and $4-2Q$ CDW satellites.

Fig. 4(a). These data were taken on X22C and are, therefore, reduced in intensity by a factor of 5 relative to the data of Fig. 2. On cooling through the Néel transition at $T\approx 311$ K, the intensity is seen to grow, reaching a maximum at $T=130$ K. At $T=120$ K, the intensity drops to half the maximum value and further cooling causes the signal to fall below background levels. This change in intensity may be readily explained in terms of the spin-flip transition at $T=122$ K. In the scattering geometry employed in these experiments, the polarization of the SDW is perpendicular to the scattering vector in the transverse phase and parallel to it in the longitudinal phase. This is illustrated in Fig. 4(b). Blume and Gibbs[37] have shown that the magnetic scattering arising from the nonresonant cross section is most sensitive to the component of the spin-density wave, which is perpendicular to the scattering plane. In this transverse SDW phase at these momentum transfers, the signal is predominantly due to this component. On passing through the spin-flip transition, the polarization aligns with Q and, for the fraction of the intensity that arises from the spin density, the ratio of the scattered intensities is[37]

$$\frac{I_{\mathrm{TSDW}}}{I_{\mathrm{LSDW}}}=\left[\frac{\sin 2\theta}{2\sin^3\theta}\right]^2\approx 42\ , \tag{1}$$

where θ is the Bragg angle. For the data of Fig. 4(a), $\theta\approx 22.2°$. From measurements of the form factor,[38] the total magnetization density is estimated to be comprised of 40% $3d$ spin density and 60% $3d$ orbital density. However, in the LSDW phase, the contribution to the scattering from the orbital magnetization is identically zero; including the orbital moments in the calculation will only serve to increase the ratio of Eq. (1). Thus, the disappearance of the signal at T_{SF} is simply explained in terms of the polarization dependence of the x-ray magnetic-scattering cross section. It is also worth noting that no change in the intensities of the $2Q$ satellites was observed on passing through T_{SF}.

From the ratio of the magnetic scattered intensity at $(Q,0,0)$ to that of the (200) charge Bragg peak, we may obtain a rough estimate of the average-ordered magnetic moment. Blume[5] estimates the ratio of the integrated intensities to be

$$\frac{I_{\mathrm{mag}}}{I_{\mathrm{charge}}}=\left[\frac{\hbar\omega}{mc^2}\right]^2\left[\frac{f_m}{f}\right]^2\frac{\langle\mu\rangle^2}{N^2}\ , \tag{2}$$

where $\hbar\omega$ is the photon energy, mc^2 is the rest mass energy of an electron, f_m and f are the magnetic and charge form factors, respectively, N is the number of electrons per atom, and $\langle\mu\rangle$ is the average moment per atom. With $\hbar\omega=6$ keV, $N=24$, $f_m(Q,0,0)/f(2,0,0)\approx 1.2$ (Refs. 27 and 39), and $I_{\mathrm{mag}}/I_{\mathrm{charge}}=3\times 10^{-8}$, we obtain $\langle\mu\rangle\approx 0.29\mu_B$ at $T=140$ K, in qualitative agreement

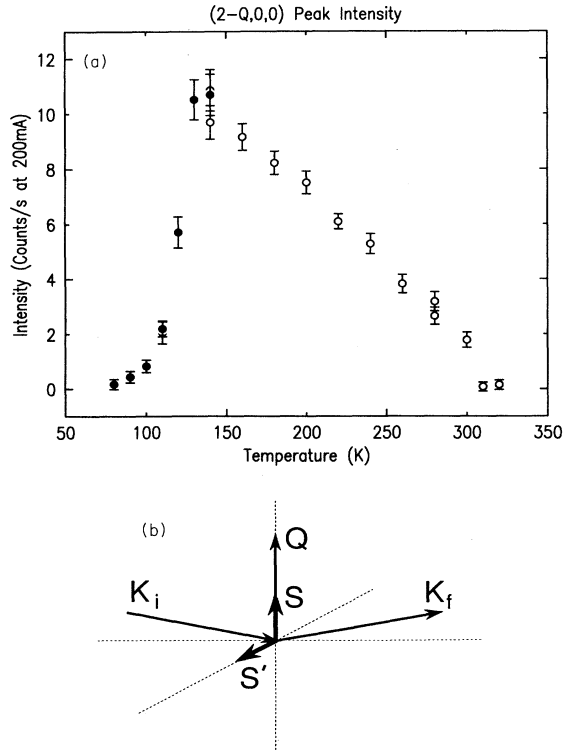

FIG. 4. (a) The intensity variation of the magnetic scattering observed at the $(2-Q,0,0)$ satellite. At $T_{\mathrm{SF}}=122$ K, the transverse polarization of the SDW is transformed to a longitudinal polarization. The sudden decrease in intensity reflects the polarization dependence of the nonresonant cross section. These data were taken on a bending magnet beamline at $E=5.978$ keV. Open circles were taken on warming from $T=140$ K, filled circles on cooling from $T=140$ K. (b) The scattering geometry. $\mathbf{K}_i$ and $\mathbf{K}_f$ are the incident and outgoing wave vectors, respectively. $\mathbf{Q}$ is the modulation wave vector and is parallel to the scattering vector. In the transverse SDW phase, the polarization is perpendicular to $\mathbf{Q}$ and the cross section is dominated by the component S'. In the longitudinal SDW phase ($T<T_{\mathrm{SF}}$) the polarization S is along $\mathbf{Q}$.

with the value obtained from neutron scattering $\langle\mu\rangle = 0.43\mu_B$ at $T = 4.2$ K.[40] For the purposes of this calculation, we have assumed that the magnetic and charge Bragg peaks are both resolution limited. In this case, the peak intensities are proportional to the scattering cross section and may be used in Eq. (2).

We also looked for resonant enhancements in the scattered intensity at $(Q,0,0)$ in the vicinity of the Cr K edge at $E = 5989$ eV. This is the only edge accessible at this momentum transfer. Large enhancements in the intensity of the magnetic scattering are possible when the incident photon energy is tuned through an atomic transition, a process known as resonant exchange scattering.[6] In such a situation, the scattering is a two-step process. The incoming photon excites a core electron into a magnetic (or exchange split) valence state, which subsequently decays via the emission of an elastically scattered, coherent photon. The size of the enhancement is determined by the lifetime of the excited state and the overlap between the core and valence levels. Particularly large enhancements have been observed at the L edges of the heavy rare-earths[7] and transition metals[25,41] and at the M edges of the actinides.[17] A weak resonance has been observed at the K edge of Ni.[20]

The measurements were performed by scanning the incident energy while moving the spectrometer angles to maintain a fixed scattering vector. The fluorescence signal was simultaneously monitored by measuring the background in the experimental hutch. The results of such energy scans, taken at X25, are shown in Fig. 5.

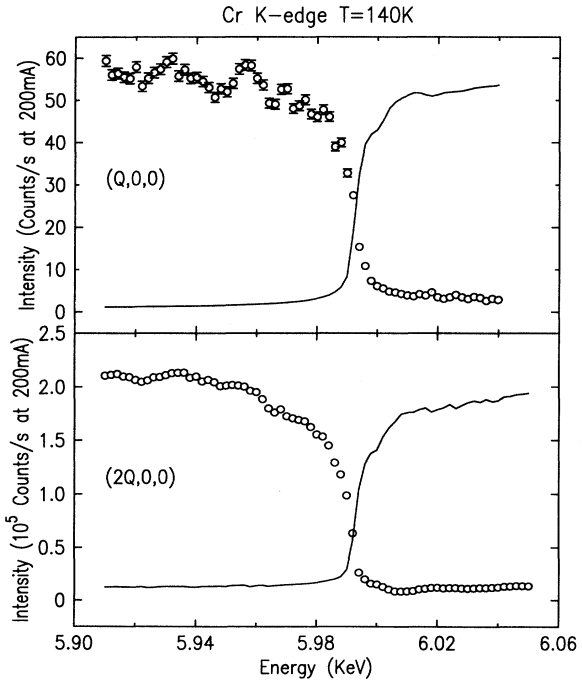

FIG. 5. The variation in the diffracted intensity at the magnetic SDW peak (top panel) and the charge CDW peak (bottom panel) as the incident x-ray energy is scanned through the Cr K edge. No resonant enhancement of the magnetic signal is observed. No corrections have been made for absorption.

The solid line denotes the fluorescence and the open circles the scattered intensity at $(Q,0,0)$. For comparison purposes, the charge scattering at $(2Q,0,0)$, where large resonant enhancements are not expected, is also shown.

Qualitatively, the intensities of both peaks are roughly constant below the edge, falling sharply as the K edge is reached and the absorption increases. Immediately above the edge, the peak remains very weak in both cases. There is no evidence of any significant enhancement of the magnetic signal in the vicinity of the K edge. This is not surprising in view of the small overlap between the highly localized $1s$ and extended $4p$ oribtals and is consistent with the weak enhancement observed at the K edge in Ni.[20]

IV. CHARGE SCATTERING

A longitudinal scan along the $(h,0,0)$ direction, parallel to the surface normal is shown in Fig. 6. These data were taken at $T = 140$ K on X22C at $E = 8000$ eV and are plotted on a semilog scale. The satellites at $q = 1.910$ and $q = 2.099$ rlu are the second harmonic, CDW satellites $(2Q,0,0)$ and $(4-2Q,0,0)$, respectively. In addition, there is a second set of satellites at $q = 1.816$ and $q = 2.194$, which may be indexed as the fourth-harmonic satellites $(\bar{2}+4Q,0,0)$ and $(6-4Q,0,0)$, respectively. From the data of Fig. 6 and similar scans, one may deduce the domain structure of the CDW state and the amplitudes of the Fourier components. We first discuss the domain structure.

It is well known from neutron-scattering experiments that pure chromium forms a "poly-Q" domain state below T_N, in which different regions of the sample select different [100] cubic axes for the direction of Q.[27] However, the entire sample may be driven into a single-Q state by cooling through the Néel transition in the presence of either a magnetic field[42,43] or a tensile stress[42] applied

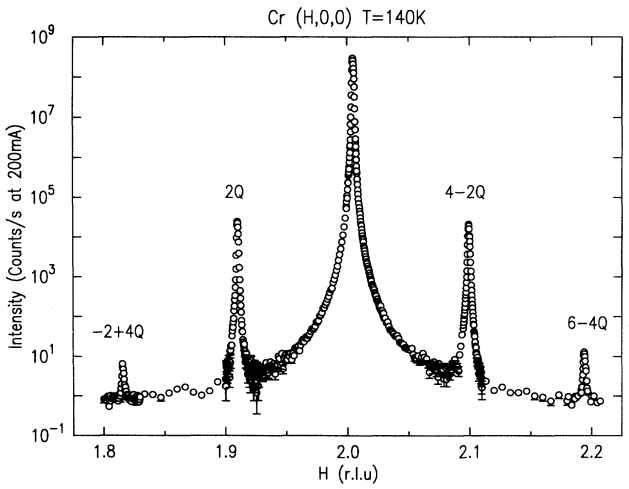

FIG. 6. A longitudinal scan in the vicinity of the (200) Bragg peak taken on a bending magnet beamline. $2Q$ and $4Q$ satellites due to the CDW are observed. Note the scale is semilogarithmic. On this scale, the magnetic intensity at $T = 140$ K is about the same magnitude as that of the $4Q$ satellite (see Fig. 4).

along a cubic axis.

A survey of the accessible satellites of the (200), (220), and (310) Bragg peaks was carried out to ascertain the domain structure of the near-surface region as probed by x rays. These experiments were undertaken at 8 keV for which the absorption length is 5.3 μm, corresponding to a penetration depth of 1.4 μm at the symmetric (200) reflection. The results are consistent with the existence of a single-Q state in this volume, with Q normal to the surface. Specifically, the satellite intensities at $(2Q,0,0)$ and $(4-2Q,0,0)$ were strong and equal to about 30 000 counts/s at a ring current of 200 mA and $T=20$ K. In contrast, the satellites at $(2,\bar{2}+2Q,0)$ and $(2,2-2Q,0)$, and $(2,0,\bar{2}+2Q)$ and $(2,0,2-2Q)$, while observable, were considerably weaker, each with intensities of ~ 2 counts/s. As discussed below, the intensity of a satellite due to a strain-wave distortion varies as $\propto[(\mathbf{q}\cdot\boldsymbol{\Delta}/2]^2$ [Eq. (4)], where $\boldsymbol{\Delta}$ is the amplitude of the sine-wave distortion and is parallel to $\mathbf{Q}$, and $\mathbf{q}$ is the momentum transfer. It follows that the off-specular satellites around the (200), which correspond to domains with Q oriented nearly perpendicular to the momentum transfer, are reduced in intensity by the geometrical factor $\sim\sin^2(0.1/2)\approx\frac{1}{400}$. Thus, if all three Q domains were equally populated, off-axis peak intensities of ~ 75 counts/s would be expected. This is significantly more than observed, which suggests that the domains with Q in the plane of the surface are underrepresented. To confirm the single-Q nature of the CDW state, the satellites around the (220) Bragg peak were studied. In this case, the geometrical factors for the satellites in the scattering plane are approximately equal. Although the intensities are weaker, because of the near-grazing angle geometry, only the $(4-2Q,2,0)$ and $(2Q,2,0)$ peaks were observable at 2500 and 350 counts/s, respectively, consistent with only Q_x domains being present. Similarly, strong peaks at $(5-2Q,1,0)$ and $(1+2Q,1,0)$ were observed. We conclude that a single-Q state exists in the near-surface region, with Q normal to the surface and that the other domains occupy $\sim 3\%$ of the probed volume. Scans of the sample across the incident beam suggests that the spatial extent of the domain structure is $\geq 1\times 1$ mm^2.

One possible origin of the single-Q state is the residual stress left from the mechanical polishing process. Bastow and Street[42] found that a tensile stress of 0.5 kg mm^{-2} was sufficient to drive a crystal into a single-Q state. However, over the small volume observed here, the required stress is likely to be significantly smaller, consistent with the lack of any observed shift in T_N from the bulk, unstrained value. In fact, the volume probed is substantially smaller than a typical domain volume in a poly-domain sample, as estimated by neutron topography, of 10^{-3}–10^{-2} cm^3.[44] It is also conceivable that the orientation of the SDW with respect to the surface plays a role. For the observed domains, the polarization lies in the plane of the surface. This is consistent with it being energetically unfavorable for the ordered moment to be oriented along the surface normal direction. Such surface anisotropy in the domain structure has been observed previously, for example, in NpAs.[45]

We now turn to a calculation of the Fourier amplitudes of the CDW. Interpreting the satellite peaks as arising solely from a static strain-wave distortion propagating through the lattice,[34] we estimate the amplitudes of the Fourier components of the strain wave from the ratio of the Bragg-peak intensity to the appropriate harmonic peak. The structure factor, $F(\mathbf{q})=\sum_j e^{i\mathbf{q}\cdot\mathbf{r}_j}$ may be calculated by writing the position of the jth atom as

$$\mathbf{r}_j=\mathbf{r}_j^0+\boldsymbol{\Delta}_2\sin(2\mathbf{Q}\cdot\mathbf{r}_j^0)+\boldsymbol{\Delta}_4\sin(4\mathbf{Q}\cdot\mathbf{r}_j^0)\ , \tag{3}$$

where $\mathbf{r}_j^0$ is the equilibrium, undistorted position and Δ_2 and Δ_4 are the second and fourth Fourier components, respectively. In the limit of Δ_2, $\Delta_4 \ll a$ one may expand the exponential and obtain, to first order in Δ_2 and Δ_4,[46]

$$F(\mathbf{q})=\delta(\mathbf{q}-\mathbf{G})+\left|\frac{\mathbf{q}\cdot\boldsymbol{\Delta}_2}{2}\right|\delta(q\pm 2Q-G)+\left|\frac{\mathbf{q}\cdot\boldsymbol{\Delta}_4}{2}\right|\delta(q\pm 4Q-G)\ . \tag{4}$$

These terms do not interfere and the observed intensities just depend on the squares of the amplitudes. Note that including higher-order corrections of order Δ_2^n and Δ_4^n in the expansion of the exponential, gives rise to additional harmonics at $2nQ$ and $4nQ$, respectively. From Eq. (4), valid in the kinematic limit, the ratio of the integrated intensity of the (200) Bragg peak to that of the $(2Q,0,0)$ satellite is

$$\frac{I_{2Q}}{I_{200}}=\left|\frac{\mathbf{q}\cdot\boldsymbol{\Delta}_2}{2}\right|^2\ , \tag{5}$$

for a single-Q state. Expression (5) ignores the difference in the Debye-Waller factors of the two peaks. Since the Q vectors differ by only 5%, and the Debye temperature is ~ 500 K, phonon contributions will be essentially identical. Phason modes, on the other hand, will contribute to the CDW Debye-Waller factor and may, in principle, be large.[47] We have assumed that the phason modes are effectively frozen at these temperatures and do not include them here. In support of this assumption, we note that measurements of the lattice distortion made at $T=20$ K gave similar results as those obtained at $T=140$ K. Equation (5) also holds only for integrated intensities. However, without a detailed knowledge of the resolution function, it is not possible to accurately calculate these. Instead, we have compared the peak intensities and adjusted the error bars to account for the fact that the CDW peak is 30% broader than the Bragg peak in the longitudinal direction. From the observed value $I_{2Q}/I_{200}=8.4\times 10^{-5}$, we find that $(\Delta_2/a)=1.5\pm 0.2\times 10^{-3}$ at $T=140$ K, where we have taken the average value as calculated from both $2Q$ peaks with appropriate error bars. This procedure averages out the q dependence of the atomic form factor, assuming it is linear over this small region of momentum transfer. This value for (Δ_2/a) agrees favorably with the neutron determination of Pynn *et al.*[33] of $1.3\pm 0.3\times 10^{-3}$ at $T=200$ K, which extrapolates to $(\Delta_2/a)=1.45\pm 0.4\times 10^{-3}$ at $T=153$ K.[27] However, it disagrees with the x-ray determination of Tsunoda *et al.* who obtained $(\Delta_2/a)=2.5\pm 0.5\times 10^{-3}$ at $T=153$ K.[35] We believe that

this discrepancy arises entirely from the latter's assumption of equal populations of the three Q domains. In fact, the observed intensity ratio of Tsunoda *et al.* is identical to ours, suggesting that their sample may also have been in a single-Q state. This explanation has been previously advanced to explain the discrepancy between the x-ray and neutron results[48] and by Tsunoda as quoted in Ref. 27.

A pure sine-wave distortion will also produce diffraction harmonics at $4Q$, as noted above. However, in this case, the intensity of the fourth harmonic will be $=\frac{1}{4}[(\mathbf{q}\cdot\Delta_2)/2^4\approx 0.5$ counts/s, much less than the observed 10 counts/s. Thus, the relatively large $4Q$ peaks signal the presence of a second Fourier component in the CDW at twice the frequency of the fundamental. The amplitude may again be calculated from the intensity ratios, from which we obtain $(\Delta_4/a)=2.8\pm0.2\times10^{-5}$, at $T=140$ K, once more averaging over the two observed satellites. We note that this implies $\Delta_4/\Delta_2=1.9\pm0.3\times10^{-2}$ at $T=140$ K, the same amplitude ratio as observed for the two magnetic harmonics, $M_3/M_1=1.8\times10^{-2}$ at $T=144$ K.[27] [This is an extrapolation of the measured ratio $1.65\pm0.05\times10^{-2}$ at $T=200$ K (Ref. 33).] It is not obvious why the two should agree. For example, it is not true for the simple case in which the CDW is proportional to the square of a SDW of the form $A\sin x+B\sin 3x$. Although both Δ_4/Δ_2 and M_3/M_1 decrease as the temperature is increased, they will remain equal as long as the mean-field scaling of the harmonics is obeyed (Sec. V). A search was carried out for the sixth harmonic at $(8-6Q,0,0)$, but no evidence for a peak was seen after counting for a total of 3 min a point. The background was 0.5 counts/s.

The width of the CDW peak, when deconvolved from the experimental resolution, provides a measure of the phase-phase correlation length of the density wave. Using the (200) Bragg peak as an upper bound on the resolution at $(2Q,0,0)$, we may obtain an upper bound on the correlation length. Fitting to a Lorentzian-squared line shape convolved with a Lorentzian-squared resolution function we find $\xi=1/\kappa=3300\pm40$ Å at $T=140$ K. This finite correlation length is smaller than that measured at the SDW, and probably represents the effect of locally pinning the phase of the CDW by defects in the lattice (impurities or strains). That the relative role of defects in pinning the phases of the spin- and charge-density waves may differ warrants comment. We speculate that the SDW, resident in the conduction electrons, may be able to adjust to the presence of defects, at least those manifested by ion core displacements, and hence preserve phase coherence. However, the same defects will pin the phase of the CDW and reduce its correlation length. One might imagine that another contributing factor is the component of the scattering at $2Q$, which arises from the density wave set up by the Coulomb repulsion between the hole surfaces. This interaction will be disrupted by charge defects, whereas the SDW, arising from a Coulomb pairing of electrons and holes of opposite spin, scatters from magnetic impurities. It seems plausible that these two mechanisms could result in different correlation lengths. If the phase coherence of the CDW is reduced, it need not correspondingly reduce that of the SDW because the coupling between the two is not linear, but quadratic. This means that, for example, a 10% reduction in the CDW order parameter would only result in a 5% reduction in the SDW order parameter.

In Fig. 7, we plot the half-width at half maximum (HWHM) of the raw (undeconvolved) data from the $(4-2Q,0,0)$ CDW and the $(Q,0,0)$ SDW peaks versus temperature. As the temperature is increased, both the CDW and SDW peaks broaden. In addition, the CDW peaks move toward the Bragg peak. For the $(2Q,0,0)$ satellite, this shift also coarsens the longitudinal resolution, complicating the analysis of the data [as was the case for the SDW at $(Q,0,0)$]. In contrast, the $(4-2Q,0,0)$ satellite, plotted in Fig. 7, moves towards the nondispersive geometry and the resolution improves. Any observed broadening cannot then be a resolution effect.

Before interpreting the temperature dependence of the peak widths, there is one other experimental artifact that must be considered. As the temperature is raised, the rate of change of the peak position increases (Fig. 3). If, in the volume probed, there is a range of effective sample temperatures (caused, for example, by a strain gradient) then for a fixed cryostat temperature a range of observed incommensurabilities will be manifested, i.e., a peak broadening. Further, as the rate of change of the peak position increases, the peak broadening increases.

To take into account such effects, we have attempted to model the temperature dependence of the CDW width as

$$\kappa(T)=\kappa_0+\frac{d(2\delta)}{dT}\Delta T\ , \tag{6}$$

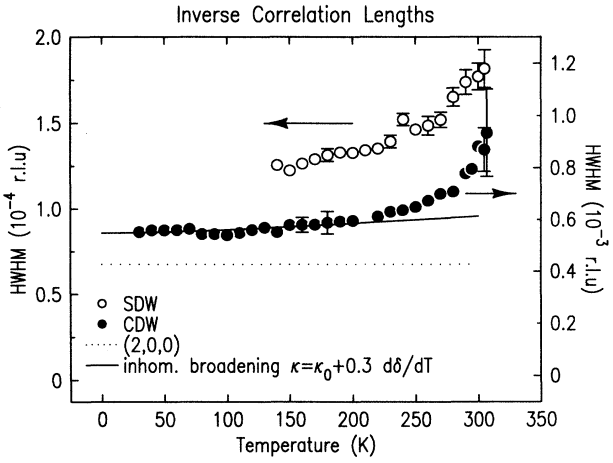

FIG. 7. Temperature dependence of the undeconvolved longitudinal widths of the $(Q,0,0)$ SDW (open circles) and the $(4-2Q,0,0)$ CDW satellites (filled circles). Note the different vertical scales, due in part to the minimum in the longitudinal resolution width near the $(Q,0,0)$ position. The solid line is a model for the broadening were it to arise from an effective temperature gradient, as discussed in the text. The dotted line represents the width of the (200) chemical Bragg peak referred to the left-hand vertical scale, and may be taken as an approximation of the resolution width at $(4-2Q,0,0)$.

where κ_0 is the low temperature width, ΔT is a constant effective temperature range, and $d\delta/dT$ is the temperature-dependent rate of change of the incommensurability, determined by numerically differentiating the peak-position data. The solid line in Fig. 7 is the result of the model calculation with $\Delta T = 0.15$ K. We find that such a description works well up to $T \approx 250$ K, but at higher temperatures the width of the $(4-2Q,0,0)$ CDW peak continues to broaden beyond that expected for a constant ΔT.

Similar line-shape broadening has been observed in the CDW compound $K_{0.3}MoO_3$ in the transverse direction, as the transition is approached from below.[49] More recently, DiCarlo *et al.* observed broadening in both longitudinal and transverse directions in Ta-doped $NbSe_3$.[50] These authors found that the transverse correlation lengths vary as the square of the order parameter, in agreement with weak pinning predictions of Fukuyama, Lee, and Rice.[51,52] They suggest that fluctuations in the Ta impurity concentration pin the phase of the CDW. As the amplitude of the CDW decreases, the relative strength of the pinning potential increases and the phase-phase correlation length decreases. It is plausible that a similar situation holds in Cr with the role of Ta impurities being played by structural defects or other impurities.

V. TEMPERATURE DEPENDENCE OF THE HARMONICS

In their original work, Pynn *et al.*[33] discovered that the intensities of the first three harmonics obeyed mean-field scaling, at least for $T \geq 220$ K. That is, the intensities of the respective harmonics follow $I_{3Q} \propto I_Q^3$ and $I_{2Q} \propto I_Q^2$. Below $T = 220$ K, the relationship continued to hold for the $2Q$ CDW satellite, but the intensity of the $3Q$ harmonic was found to saturate.[33] These workers understood the origin of the harmonics of the SDW in terms of a phenomenological Landau expansion of the free energy. Retaining only the symmetry allowed couplings between the independent order parameters, M_1, Δ_2, and M_3, and minimizing with respect to these amplitudes, leads to the mean-field scaling $I_{nQ} \propto I_Q^n$ for small M_1.

With the discovery of the $4Q$ harmonic reported above, we are presented with the opportunity of testing this scaling to the next order of the Landau expansion. In Fig. 8, we plot the intensities of the $4Q$ and $2Q$ satellites raised to the appropriate power, together with the neutron-scattering data of Werner, Arrot, and Kendrick[53] for the fundamental SDW satellite taken on a single-Q sample. These data have been normalized to unity at $T = 150$ K and, where appropriate, a small constant temperature offset has been included to allow for differences in the thermometry of the various data sets. (In all cases, this was less than 2 K.) As may be seen from the figure, the $4Q$ harmonic, unlike the $3Q$ harmonic, appears to obey mean-field scaling down to $T = 140$ K, the lowest temperature studied in this aspect of the work. The unscaled intensities are plotted in the inset of Fig. 8, and demonstrate that the density wave becomes more sinusoidal as the temperature is raised.

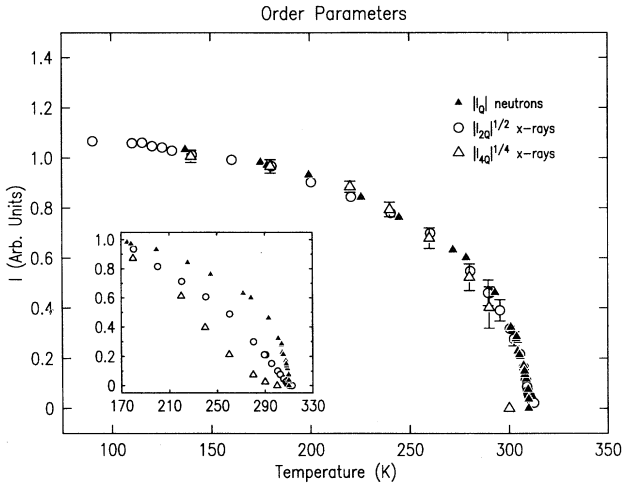

FIG. 8. Scaling plot of the order parameters. The filled triangles are the neutron-scattering data of Ref. 53 taken at $(Q,0,0)$ on a single Q sample and normalized to unity at $T = 150$ K. The open circles represent the intensity of the second-harmonic CDW, again normalized to unity and raised to the power 0.5. The open triangles are the fourth harmonic, similarly normalized and raised to the power 0.25. Such simple scaling of the harmonics is predicted within mean-field theory. The inset shows the unscaled intensities normalized to unity at $T = 150$ K.

Interestingly, the x-ray magnetic-scattering intensities (Fig. 4) do not have the temperature dependence of Fig. 8, although they are in approximate agreement with magnetic neutron data taken on multi-Q samples of chromium.[54,55] Such a discrepancy between multi-Q and single-Q temperature dependences is well known and has been attributed to a redistribution of the spectral weight between the magnetic satellites.[53] If correct, this explanation implies that the x rays probe a multi-Q state at $(Q,0,0)$ for which the penetration depth is 3.9 μm at 6 keV and a single-Q state at $(2Q,0,0)$ when the penetration depth is 1.4 μm at 8 keV. In principle, this idea could be tested by comparing the temperature dependence of the order parameter obtained for reflections at large and small momentum transfer, corresponding to larger and smaller penetration depths, and as a function of incident photon energy.

It is worthwhile to compare the scaling of the harmonics in chromium with other systems with incommensurate modulations. We collect here some recent results and note the appropriate universality class, as determined by the dimensionality of the order parameter n and the spatial dimension d. Together with chromium ($n = 12$, $d = 3$), mean-field scaling has been observed in the c-axis modulated magnetic structures ($n = 2$, $d = 3$) of erbium[56] and thulium.[56,11] In contrast, there are a number of systems that exhibit nonclassical scaling. These include the spiral antiferromagnets ($n = 4$, $d = 3$) holmium[16] and dysprosium,[56] and two incarnations of the $3d$ XY ($n = 2$, $d = 3$) universality class, Rb_2ZnCl_4 (Ref. 57) and the smectic liquid crystal 7APCBB.[58] All these latter systems have been found to obey the $3d$ XY mulitcritical scaling

theory of Aharony *et al.*, developed originally to model the smectic-I to hexatic transition of the liquid crystal 8OSI.[59,60] In this theory, $I_n \propto I_1^{\sigma_n}$ and $\sigma_n = n + \lambda n(n-1)$ where $\lambda \approx 0.3$ for the $3d$ XY model and empirically $\lambda = 0.22$ for the $n=4$, $d=3$ systems.[16,56]

We conclude this section by noting that the intensity of the CDW satellite is unchanged on cooling through the spin-flip transition at $T_{SF} \approx 120$ K (open circles in Fig. 8). In addition, the width of the scattering remains constant through T_{SF} (Fig. 7). Such continuous behavior has been observed previously[48] and stands in contrast to the first-order nature of the transition. It may shed light on the nature of the spin-flip transition (see, for example, Ref. 61).

VI. SUMMARY

We have carried out a high-resolution x-ray scattering study of the density waves of pure chromium. We observe magnetic scattering at the first harmonic, which disappears in the longitudinal SDW phase, consistent with the polarization dependence of the x-ray magnetic-scattering cross section. From the intensities of the various second-harmonic peaks, we have determined the near-surface region (~ 1 μm) exists in an almost single-Q state. The calculated amplitudes of the lattice distortion are in good agreement with published values from neutron-scattering experiments. A fourth harmonic of the density wave is observed, and suggests that the CDW, like the SDW, is not a pure sine wave. The temperature dependence of the observed charge harmonics obey mean-field scaling, unlike a subset of other incommensurate systems.

ACKNOWLEDGMENTS

We thank J. Bohr for the loan of one of the samples used in this work and L. Berman for his assistance at X25. Stimulating conservations with J. D. Brock, R. S. Fishman, R. M. Fleming, S. E. Nagler, P. Sonntag, and B. J. Sternlieb, who also participated in some of the experiments, are gratefully acknowledged. G.H. would like to thank the research council of Norway for partial financial support. The work was supported by the U.S. Department of Energy, Division of Materials Science under Contract No. DE-AC02-76CH00016.

*Present address: Institutt for Energiteknikk, N-2007 Kjeller, Norway.

[1]F. de Bergevin and M. Brunel, Phys. Lett. A **39**, 141 (1972).

[2]F. de Bergevin and M. Brunel, Acta. Crystallogr. Sec. A **37**, 314 (1981).

[3]M. Brunel and F. de Bergevin, Acta. Crystallogr. Sec. A **37**, 324 (1981).

[4]P. Platzman and N. Tzoar, Phys. Rev. B **2**, 3556 (1970).

[5]M. Blume, J. Appl. Phys. **57**, 3615 (1985).

[6]J. P. Hannon, G. T. Trammel, M. Blume, and D. Gibbs, Phys. Rev. Lett. **61**, 1245 (1988).

[7]D. Gibbs, D. R. Harshmann, E. D. Isaacs, D. B. McWhan, D. Mills, and C. Vettier, Phys. Rev. Lett. **61**, 1241 (1988).

[8]D. Gibbs, G. Grubel, D. R. Harshmann, E. D. Isaacs, D. B. McWhan, D. Mills, and C. Vettier, Phys. Rev. B **43**, 5663 (1991).

[9]D. Gibbs, D. E. Moncton, K. L. D'Amico, J. Bohr, and B. H. Grier, Phys. Rev. Lett. **55**, 234 (1985).

[10]D. Gibbs, J. Bohr, J. D. Axe, D. E. Moncton, and K. L. D'Amico, Phys. Rev. B **34**, 8182 (1986).

[11]J. Bohr, D. Gibbs, and K. Huang, Phys. Rev. B **42**, 4332 (1990).

[12]E. D. Isaacs, D. B. McWhan, P. Siddons, J. B. Hastings, and D. Gibbs, Phys. Rev. B **40**, 9336 (1989).

[13]M. K. Sanyal, D. Gibbs, J. Bohr, and M. Wulff, Phys. Rev. B **49**, 1079 (1994).

[14]D. B. Pengra, N. B. Thoft, M. Wulff, R. Feidenhans'l, and J. Bohr, J. Phys. C **6**, 2409 (1994).

[15]C. Vettier, D. B. McWhan, E. M. Gyorgy, J. Kwo, B. M. Buntschuh, and B. W. Batterman, Phys. Rev. Lett. **56**, 757 (1986).

[16]G. Helgesen, J. P. Hill, T. R. Thurston, D. Gibbs, J. Kwo, and M. Hong, Phys. Rev. B **50**, 2990 (1994).

[17]E. D. Isaacs *et al.*, Phys. Rev. Lett. **62**, 1671 (1989).

[18]E. D. Isaacs, D. B. McWhan, R. N. Kleinman, D. J. Bishop, G. E. Ice, P. Zschack, B. D. Gaulin, T. E. Mason, J. D. Garrett, and W. J. L. Buyers, Phys. Rev. Lett. **65**, 3185 (1990).

[19]C. C. Tang, W. G. Stirling, G. H. Lander, D. Gibbs, W. Herzog, P. Carra, B. T. Thole, K. Mattenberger, and O. Vogt, Phys. Rev. B **46**, 5287 (1991).

[20]K. Namikawa, M. Ando, T. Nakajima, and H. Kawata, J. Phys. Soc. Jpn. **54**, 4099 (1985).

[21]A. I. Goldman, K. Mohanty, G. Shirane, P. M. Horn, R. L. Greene, C. J. Peters, T. R. Thurston, and R. J. Birgeneau, Phys. Rev. B **36**, 5609 (1987).

[22]T. R. Thurston, C. J. Peters, R. J. Birgeneau, and P. M. Horn, Phys. Rev. B **37**, 9559 (1988).

[23]J. P. Hill, Q. Feng, R. J. Birgeneau, and T. R. Thurston, Z. Phys. B **92**, 285 (1993).

[24]F. de Bergevin, M. Brunel, R. M. Galera, C. Vettier, E. Elkaim, M. Besseière, and S. Lefèbvre, Phys. Rev. B **46**, 10 772 (1992).

[25]J. M. Tonnerre, M. Jergel, D. Raoux, M. Idir, G. Soullier, R. Barchewitz, and B. Rodmacq, J. Magn. Magn. Mater. **121**, 230 (1993).

[26]D. Gibbs, Synchrotron Radiat. News **5**, 18 (1992).

[27]E. Fawcett, Rev. Mod. Phys. **60**, 209 (1988).

[28]A. Overhauser, Phys. Rev. Lett. **4**, 226 (1960).

[29]A. Overhauser, Phys. Rev. **128**, 1437 (1962).

[30]The polarization of the conduction electrons reverses with a period of $\frac{26}{27}$ lattice constants at T_N (wave vector, $Q=0.963$). This means one must travel 27 lattice constants before the polarization is identical in magnitude and direction at an equivalent point on the lattice. The modulation may be equivalently described by a wave vector Q or $\delta = 1-Q$, which are trivially related.

[31]L. M. Corliss, J. M. Hastings, and R. J. Weiss, Phys. Rev. Lett. **3**, 211 (1959).

[32]V. N. Bykov, V. S. Golovkin, N. V. Ageev, V. A. Levdik, and S. I. Vinogradov, Dokl. Akad. Nauk SSSR **4**, 1149 (1959). [Sov. Phys. Dokl. **128**, 1070 (1959)].

[33]R. Pynn, W. Press, S. M. Shapiro, and S. A. Werner, Phys. Rev. B **13**, 295 (1976).

[34]Conceptually, there are two mechanisms for producing a den-

sity wave in the charge distribution. First, the lattice may be periodically distorted, with each ion retaining its equilibrium charge (a strain wave). Second, there may be a periodic excess and deficit of charge on the sites of an undistorted lattice. In the CDW literature, these two effects are collectively referred to as charge-density waves. Both produce x-ray diffraction peaks and in this work we do not distinguish between the two contributions at $\pm 2Q$ and $\pm 4Q$, referring to both satellites as CDW peaks. The dominant contribution to the x-ray intensity arises from the core electrons (the strain wave). An attempt has been made to separate the two contributions [M. Mori and Y. Tsunoda, J. Phys. C **5**, L77 (1993)]. The x-ray intensity was found to be largely due to the lattice distortion and a small additional conduction-electron density wave was claimed.

[35]Y. Tsunoda, M. Mori, N. Kunitomi, Y. Teraoka, and J. Kanamori, Solid State Commun. **14**, 287 (1974).

[36]D. Gibbs, K. M. Mohanty, and J. Bohr, Phys. Rev. B **37**, 562 (1988).

[37]M. Blume and D. Gibbs, Phys. Rev. B **37**, 1779 (1988).

[38]C. Stassis, G. R. Kline, and S. K. Sinha, Phys. Rev. Lett. **31**, 1498 (1973).

[39]B. E. Warren, *X-Ray Diffraction* (Dover, New York, 1990).

[40]A. Arrott, S. A. Werner, and H. Kendrick, Phys. Rev. **153**, 624 (1967).

[41]A. Garrett, J. F. Ma, J. Zhang, S. E. Nagler, D. F. McMorrow, T. R. Thurston, and E. D. Isaacs, Bull. Am. Phys. Soc. **39**, 531 (1994).

[42]T. J. Bastow and R. Street, Phys. Rev. **141**, 510 (1966).

[43]A. Arrott, S. A. Werner, and H. Kendrick, Phys. Rev. Lett. **14**, 1022 (1965).

[44]M. Ando and S. Hosoya, Phys. Rev. Lett. **29**, 281 (1972).

[45]S. Langridge, W. G. Stirling, G. H. Lander, and J. Rebizant, Phys. Rev. B **49**, 12 010 (1994).

[46]The exact expression for the structure factor derived using the generating function for Bessel functions $e^{iz\sin\phi}=\sum_n e^{in\phi}J_n(z)$ reduces to Eq. (4) in the small distortion limit (Ref. 47).

[47]A. Overhauser, Phys. Rev. B **3**, 3173 (1971).

[48]C. F. Eagen and S. A. Werner, Solid State Commun. **16**, 1113 (1975).

[49]R. M. Fleming, R. G. Dunn, and L. F. Schneemeyer, Phys. Rev. B **31**, 4099 (1985).

[50]D. DiCarlo, R. E. Throne, E. Sweetland, M. Sutton, and J. D. Brock, Phys. Rev. B **50**, 8288 (1994).

[51]H. Fukyama and P. A. Lee, Phys. Rev. B **17**, 535 (1978).

[52]P. A. Lee and T. M. Rice, Phys. Rev. B **19**, 3970 (1979).

[53]S. A. Werner, A. Arrott, and H. Kendrick, Phys. Rev. **155**, 528 (1967).

[54]G. Shirane and W. J. Takei, J. Phys. Soc. Jpn. **17**, Suppl. B (1962).

[55]J. P. Hill, G. Helgesen, G. Shriane, and D. Gibbs (unpublished).

[56]G. Helgesen, J. P. Hill, T. R. Thurston, and D. Gibbs (unpublished).

[57]M. Zinkin, D. F. McMorrow, J. P. Hill, A. Gibaud, and R. A. Cowley (unpublished).

[58]L. Wu, M. J. Young, Y. Shao, C. W. Garland, R. J. Birgeneau, and G. Heppke, Phys. Rev. Lett. **72**, 376 (1994).

[59]J. D. Brock, A. Aharony, R. J. Birgeneau, K. W. Evans-Lutterodt, J. D. Litster, P. M. Horn, G. B. Stephenson, and A. R. Tajbakhsh, Phys. Rev. Lett. **57**, 98 (1986).

[60]A. Aharony, R. J. Birgenau, J. D. Brock, and J. D. Litster, Phys. Rev. Lett. **57**, 1012 (1986).

[61]W. Cowan, J. Phys. F. **8**, 423 (1978).